Proposal for practical multidimensional quantum networks

Davide Bacco,[1,*] Jacob F. F. Bulmer,[2] Manuel Erhard,[3,4] Marcus Huber,[4,5,6] and Stefano Paesani[7]

[1]*CoE SPOC, DTU Fotonik, Technical University of Denmark, 2800 Kongens Lyngby, Denmark*
[2]*Quantum Engineering Technology Labs, University of Bristol, Bristol BS8 1FD, United Kingdom*
[3]*Vienna Center for Quantum Science & Technology (VCQ),Faculty of Physics, University of Vienna, 1090 Wien, Austria*
[4]*Quantum Technology Laboratories (qtlabs) GmbH, Wohllebengasse 4/4 1040 Vienna, Austria*
[5]*Institute for Atomic and Subatomic Physics, Vienna University of Technology, 1020 Wien, Austria*
[6]*Vienna Center for Quantum Science and Technology, Atominstitut, TU Wien, 1020 Vienna, Austria*
[7]*Center for Hybrid Quantum Networks (Hy-Q), Niels Bohr Institute, University of Copenhagen, 2100 Blegdamsvej, Denmark*

(Received 31 May 2021; revised 7 October 2021; accepted 2 November 2021; published 23 November 2021)

A quantum internet, i.e., a global interconnection of quantum devices, is the long-term goal of quantum communications and has so far been based on two-dimensional systems (qubits). Recent years have seen a significant development of high-dimensional quantum systems (qudits). While qudits present higher photon information efficiency and robustness to noise, their use in quantum networks presents experimental challenges due to the impractical resources required in high-dimensional quantum repeaters. Here, we show that such challenges can be met via the use of standard quantum optical resources, such as weak coherent states or weak squeezed states, and linear optics. We report a concrete design and simulations of an entanglement swapping scheme for three- and four-dimensional systems, showing how the network parameters can be tuned to optimize secret key rates and analyzing the enhanced noise robustness at different dimensions. Our work significantly simplifies the implementation of high-dimensional quantum networks, fostering their development with current technology.

DOI: 10.1103/PhysRevA.104.052618

I. INTRODUCTION

The advent of quantum information has strongly influenced modern technological progress. Intense research activities have been carried out in the last two decades, producing outstanding results in fields such as, e.g., quantum computing [1], quantum communication [2–6], and quantum simulation [7,8] with the final goal of realizing a quantum computer and a quantum internet. The quantum computer will, for example, enable accurate simulations of chemical and biological compounds, while the quantum internet will allow communication between users (either classical or quantum) guaranteeing multiple applications, from secure communications to remote quantum computing [9,10].

Both in the quantum computer infrastructure and in the quantum internet, it is crucial to transport quantum states, i.e., perform quantum communications, either between components in the same quantum device [11] or between nodes in a network [12]. Independently from the technology which will master the challenge of realizing the quantum computer, photons are the only candidates for transmitting quantum information over long distances [3,4]. In the case of continental applications, these photons are easily transportable by optical fibers, and since this medium is already deployed worldwide in the context classical communication, the quantum community plans to reuse the same fiber infrastructure. Unfortunately, the transmission of photons, over long distances, is limited by the intrinsic loss of the optical fibers, and by the external noise due to the interaction with the outside environment, which destroys the quantum states. Another hurdle comes from central laws of physics, which state the infeasibility of creating an identical copy of an arbitrary unknown quantum state [13]. A solution to these problems is provided by quantum repeaters (QRs), i.e., the quantum counterpart of classical repeaters [14–17]. Different kinds of quantum repeater protocols can be identified and are usually classified into three distinct categories or generations (first generation, quantum memory and purification protocol; second generation, quantum repeater with error correction against operational errors; third generation, fully fault-tolerant quantum repeaters [15,16,18]). Current quantum repeater proposals mainly rely on a two-dimensional encoding scheme (*qubit*) as an information unit, which due to the decoherence processes, caused by interaction with the external environment, lose their ability to stay in superposition and/or in an entangled state. This can be directly translated to a limited robustness to noise and thus limit the overall applicability.

A potential workaround is provided by high-dimensional quantum states (qudits), which offer an intrinsic advantage in terms of photon information efficiency and robustness to noise [19,20]. In recent years many advances towards the development of high-dimensional (Hi-D) quantum networks have been achieved. High-quality generation and manipulation of high-dimensional entangled states have been demonstrated using the orbital angular momentum (OAM), time-bin, frequency, and path degrees of freedom using bulk or fiber optics, as well as in integrated quantum photonics [21]. Low-loss

*dabac@fotonik.dtu.dk

 ©2021 American Physical Society

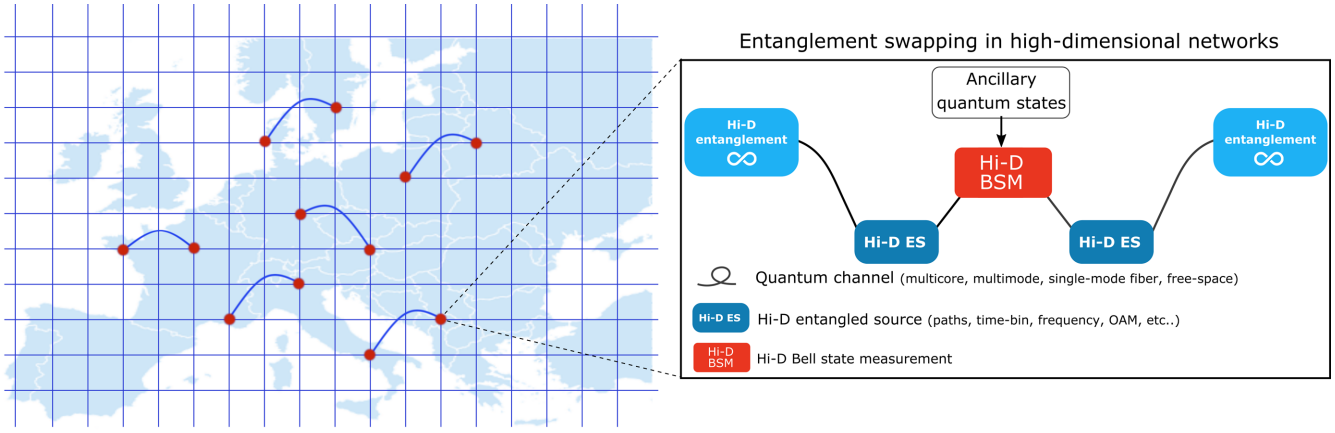

FIG. 1. Imaginative view of a multidimensional quantum network. The inset describes a potential building block of such a network. Two sources of entangled photons (cyan boxes) emit high-dimensional quantum states which are propagated through different quantum channels. An intermediate node (red box) measures the two multidimensional photons using ancillary quantum states. Once the Hi-D quantum interference generates a positive outcome, multidimensional entanglement is generated between the two users (light blue boxes).

transmission of high-dimensional states has been reported through fiber and free-space with high fidelities [22].

However, the realization of high-dimensional quantum repeaters has remained an open experimental challenge mainly due to the lack of schemes for Bell measurements in higher dimensions, i.e., a fundamental action in the quantum repeater schemes. Indeed, it has been proved that, without ancillary photons, the projection into a high-dimensional Bell state is unattainable with only linear optics [23]. Very recently, two different schemes have been proposed to perform linear-optical Bell measurements in high dimensions with the use of ancillary single photons and have been demonstrated for $d = 3$ [24,25]. However, the lack of deterministic single-photon sources makes the requirements of such ancillary single photons a stringent hurdle for current technologies, limiting the practicability of developing high-dimensional quantum networks.

Here, we show that schemes for high-dimensional Bell measurements can operate with high fidelity, using practical resources: weak-coherent states and sources of weak squeezing. We numerically test the performances of this scheme for realistic quantum repeaters by developing a simulator of the Gaussian resources and evolutions employed, and single-photon measurements with the use of threshold detectors (which distinguish between vacuum and nonvacuum outcomes). Even though the experimental resources are significantly simplified, we numerically identify regimes where high-dimensional quantum states offer advantages in entanglement-based quantum network protocols. Our proposal paves the way for a practical implementation of high-dimensional quantum states in future quantum networks.

II. PROTOCOLS

Future quantum networks will be constituted of quantum nodes (i.e., repeater station) where nonclassical correlation will be shared between different users. In order to achieve this goal, it is possible to define three main operations, which are reported in Fig. 1: generation, transmission, and interference of high-dimensional quantum states. Regarding the generation and transmission of Hi-D quantum states, an increasing number of demonstrations have been achieved during the last five years. However, Hi-D Bell state measurement (BSM) remains still challenging due to its limited practicability and efficiency.

Linear-optical circuit for Bell measurements in high dimensions. Let us consider the simplest building block for a quantum network based on high-dimensional quantum states, as depicted in Fig. 1. The goal is to extend the achievable distance by connecting two high-dimensional entangled quantum states with a repeater. Here we envision the simplest quantum repeater, an optical Bell measurement.

An optical Bell measurement is a detectable projection of two single photons into a maximally entangled Bell state. For two-dimensional photons, the Bell measurement can be performed by a single beam-splitter and two single-photon detectors at the outputs. The trick is to utilize two-photon interference at a 50/50 beam-splitter, namely, Hong-Ou-Mandel interference, and detect the two photons simultaneously after the beam-splitter in two different outputs. If such an event occurs, we know that the two photons have been projected into an asymmetric Bell state at the beam-splitter. This Bell measurement is the key part of every photonic quantum teleportation or entanglement-swapping experiment as it can entangle two photons that have never interacted before.

Luo *et al.* [24] extended these ideas and proposed a generalized BSM in higher dimensions. They replaced the beam-splitter with a generalized Fourier-transform interferometer (FTI). The FTI interferes with different photons $\{a, b, c, d\}$ that all occupy the same mode m, e.g., $|1\rangle_a|1\rangle_c|1\rangle_d|1\rangle_b$, as depicted in Fig. 2, according to

$$|m\rangle_p \to \frac{1}{\sqrt{d}} \sum_{\ell\in\{b,c,d,e\}} \exp\left[m\frac{2\pi i}{d}\Phi(p)\right]|m\rangle_\ell, \qquad (1)$$

with $\Phi(p)$ denoting a path-dependent phase (see Appendix A). The FTI is a linear operation, but using linear optics only is not sufficient to project two photons into a d-dimensional Bell state [23]. Therefore, $d-2$ ancillary

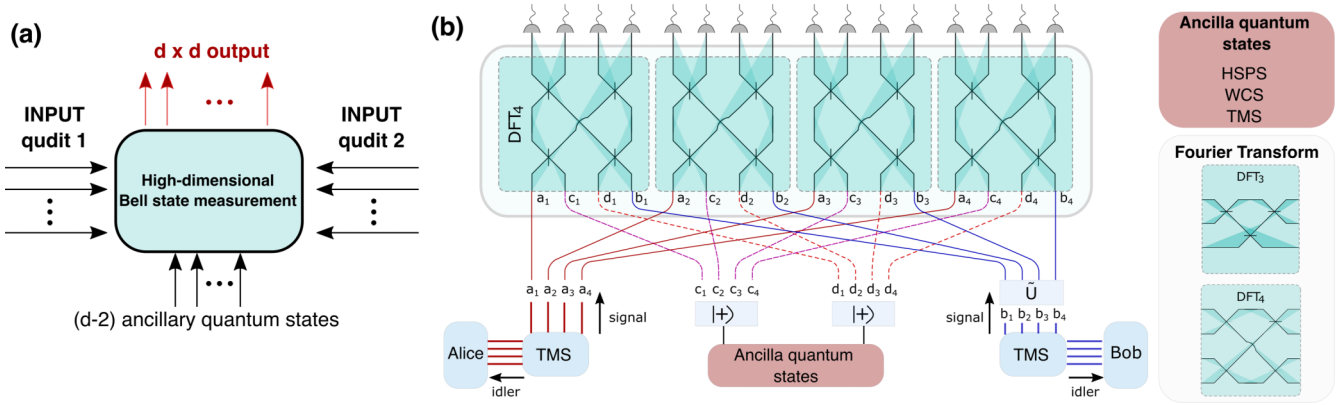

FIG. 2. Scheme of the high-dimensional quantum interference with linear optics. (a) Overview scheme. Input 1 and input 2 are the two high-dimensional quantum states encoded in path degrees of freedom (d-dimensionality of the Hilbert space). The scheme requires $d-2$ ancillary quantum states and d^2 outputs for a complete measurement. (b) Overview scheme. Detailed setup for the high-dimensional Bell state measurements (BSM). TMS, two-mode squeezed state; WCS, weak coherent state; HSPS, heralded single-photon source; DFT_n, discrete Fourier transform in an n-dimensional system.

photons are added to the protocol. Finally, an extended unitary transformation in U_{4+1} dimensions combined with postselection of specific detection click-patterns is performed. Note that in d-dimensional Hilbert space, $d \times d$ outputs are required. Observing these click-patterns indicates the unambiguous projection of the two incoming photons into a four-dimensional Bell state. This completes the four-dimensional entanglement swapping protocol; further details are presented in Appendix A. To perform Bell measurements in dimension d, we here only use the d heralding patterns that are known to provide perfect correlations after the entanglement swapping [24]. However, we note that many other heralding patterns are possible, resulting in high-dimensional entanglement being shared between the parties, although not maximally entangled. These could be used to significantly boost the success probability of the Bell measurement (see Appendix A).

Practical ancillary quantum states. Since the deterministic generation of single photons in high dimensions at 1550 nm is still an open challenge, we have proposed the possibility of replacing the ancillary single photons with ancillary quantum states which are easier to generate. As reported in Fig. 2, we consider three different kind of quantum states for the ancillas: weak coherent states (WCS), two-mode squeezed states (TMS), and heralded single-photon sources (HSPS).

In particular, in the case of three-dimensional systems, we propose to use weak coherent states generated from an attenuated laser. If the photon number per pulse is lower than 1, on average we can approximate the weak coherent states with a single photon and successfully reveal the Hi-D swapping scheme.

Weak coherent states cannot, however, be applied to four-dimensional quantum states. In fact, because in the four-dimensional Hi-D Bell measurement the number of additional particles needed is two, if two separate WCS are used the probability that two ancillary photons are generated is less than the probability of having two photons in just a single ancillary mode. The multiphoton contamination, thus, becomes significant in this scenario and reduces the measurement fidelity. However, we can exploit the photon-number correlations in two-mode squeezed states to mitigate such multiphoton noises between the two ancillary inputs. In fact, in the low squeezing regime, a TMS state approximates the ideal pair of ancillary photons with no intramode multiphoton contamination. Furthermore, the generation of a weakly squeezed quantum state is practical and experimentally simple to realize using both bulk and integrated optics [26].

Furthermore, for both $d=3$ and $d=4$, another possibility is to use heralded single photons from a TMS source as ancillas [27]. Note that HSPS can be also used with higher dimensionalities, but require twice the number of photons compared to the WC or TMS configurations considered above.

We now have introduced the main building block of a single repeater quantum communication protocol based on high-dimensional quantum states and practical ancillary resources. We will now investigate the performance of the different systems as a function of the dimensionality of the Hilbert space.

III. PERFORMANCE SIMULATION

Efficient scheme simulator. In order to simulate the performance of a practical high-dimensional quantum network, we simulate the linear-optical circuit described in Fig. 2 including the cases where two-mode squeezing, weak coherent, or heralded single-photon states are used for the ancillas, and threshold detectors (non-number-resolving) are used at the outputs. To perform a faithful simulation of all noises, and in particular multiphoton contamination from squeezed and weak-coherent states, we perform no truncation on the photon numbers in the states but rather describe their full photon statistics via the Gaussian formalism [28]. A first challenge when building the simulator is that, when increasing the dimensionality d, the total number of photons increases significantly. This makes the calculation of the output detection probabilities rapidly inefficient for classical computers as the system size is increased. To maintain a good efficiency, we exploited the fact that, prior to the detection, we only use processes which have Hamiltonians that are at

most quadratic in creation and annhilation operators. This means the states can be represented by multivariate Gaussian quasiprobability distributions in phase space, allowing for time- and memory-efficient exact simulation [28]. The non-Gaussian measurement with threshold detectors can then be simulated adapting techniques from Gaussian boson sampling [29]. In particular, to include weak-coherent states as possible inputs, we adopt a generalization of the Torontonian function used in Gaussian boson sampling to calculate output threshold detection probabilities for squeezed states [30], for the case where nonzero displacement is present [31]. Using this approach we are able to simulate qudit Bell measurement circuits with up to >20 detector clicks on a standard laptop, which we estimate to be compatible with high-dimensional quantum networks with a dimensionality exceeding $d = 15$. This is fast enough to perform a detailed analysis of the circuits studied here.

Entanglement-based quantum key distribution through the network. One of the most basic quantum communication protocols is quantum key distribution (QKD), in which two users generate a shared string of private random numbers. Using entanglement for this task unlocks the potential for device-independent security and makes the system impervious to attacks on the source. Just as for qubits, the high-dimensional protocol for QKD works on the same principle: random local measurements are performed in multiple rounds on a shared entangled state. The rounds are divided into key rounds (in a predefined computational basis with high correlations) and test rounds (in multiple incompatible bases) for estimating privacy and the need for further classical error correction. While entanglement in high dimensions is highly robust to noise, error correction in noisy states could still obliterate the actual key rates. Here, a recent protocol [32] provides a workaround: simultaneously using multiple low-dimensional subspaces keeps the advantages of noise robust entanglement, while limiting error correction to lower-dimensional subspaces. In our work, we used the simultaneously coding technique for estimating the secret key rate between Alice and Bob for different Hilbert space dimensionalities. In particular, we evaluate the performance of our system as a function of the cross-talk parameter θ. The secret key rate per round, in the asynthotic regime, has been calculated according to the following equation:

$$K \geqslant H(X|E_T) - H(X|Y), \tag{2}$$

where $H(X|E_T)$ is the von Neumann entropy of Alice's key round outcome X conditioned on the total information available to the eavesdropper Eve at the end of the parameter estimation procedure and $H(X|Y)$ is the conditional Shannon entropy between Alice's and Bob's key round outcomes [32].

Optimizing key rates for high-dimensional network. In our proposal, the photons encoding the high-dimensional entangled states as well as the ancillary ones are generated probabilistically via TMS or coherent states. We define s as the two-mode squeezing parameters at the Alice and Bob entanglement sources, and ξ (α) as the squeezing (displacement) parameter used for the ancillary photons. All these parameters affect the total key rate obtained from Alice and Bob after the high-dimensional entanglement swapping in two contrasting ways. On one hand, larger values indicate higher probabilities of generating photons, thus initially increasing the rate. On the other hand, if the squeezing or displacement parameters are too large, multiphoton contamination becomes significant, amplifying noises and decreasing the effective fidelity of the shared state after entanglement swapping, reducing the secure key rate. A central feature in the scheme is, thus, finding the optimal trade-off between these two processes, finding the parameters for Alice's and Bob's sources and ancillary photons that optimize the total key rate.

In Fig. 3, we numerically investigate the optimization for the networks in dimensions $d = 3$ and $d = 4$. The key rate is obtained from the simulator for different values of the parameters, types of ancillary states, and encoding subspaces. It can be observed that the source and ancilla parameters affect the rate in different ways, which also depends on the dimensionality and types of ancillas and encodings. The optimization is thus nontrivial for each configuration. Moreover, more noise-robust configurations can be achieved by encoding the quantum information in a subspace of dimension k (with $k \leqslant d$) of a high-dimensional system [32]. For example, one can encode a two-dimensional ($k = 2$) qubit in the subspace of a $d = 4$ system spanned by $\{|0\rangle, |3\rangle\}$ [33]. Interestingly, the higher noise robustness of these configurations, in particular, the $k = 2$ dimensional subspace encoding for $d = 4$, allows us to use higher squeezing parameters before multiphoton noises become significant, which significantly improves the optimal key rates.

Noise robustness. One of the main features of high-dimensional QKD systems is an improved noise robustness compared to qubit-based systems [19]. In order to identify regimes where the high-dimensional entanglement swapping scheme outperforms simpler qubit networks, it is important to analyze how performances are affected by realistic noises of practical relevance. We numerically investigate this by simulating noises coming from unitary linear-optical errors. In particular, we consider a crosstalk model which can arise, for example, due to intermode contamination when transmitting OAM- and path-encoded qudits through fibers [22,34]. In this model, Alice's and Bob's idler photons [see Fig. 2(b)] undergo an additional unitary evolution $\hat{U} = \exp(-i\hat{H}\theta)$, where $\hat{H} = \sum_{i=0}^{d-1} |i\rangle\langle i+1 \mod d| + \text{H.c.}$ is a nearest-neighbor coupling Hamiltonian and the crosstalk parameter $\theta \in [0, \infty)$ embeds both the crosstalk coupling strength and the coupling length.

In the presence of noise, we observe a change in the optimal source parameters which change for the noise level, as described in Fig. 3. Therefore, for a given characterized level of noise, new optimal source parameters have to be calculated. In Fig. 4 we show the secure key rates per round, optimized over the source parameters, for different levels of crosstalk and dimensions. For low levels of noise the qubit-based entanglement swapping provides better rates compared to high-dimensional systems, due to the higher Bell-measurement success probability. However, using high-dimensional systems becomes advantageous due to their higher noise robustness. In fact, increasing the dimensionality allows us to achieve secure keys even in regimes where qubit-based schemes are no longer secure, although at lower rates. In particular, the $d = 4$ and $k = 2$ configuration shows good rates even for very high levels of noises, which is promising

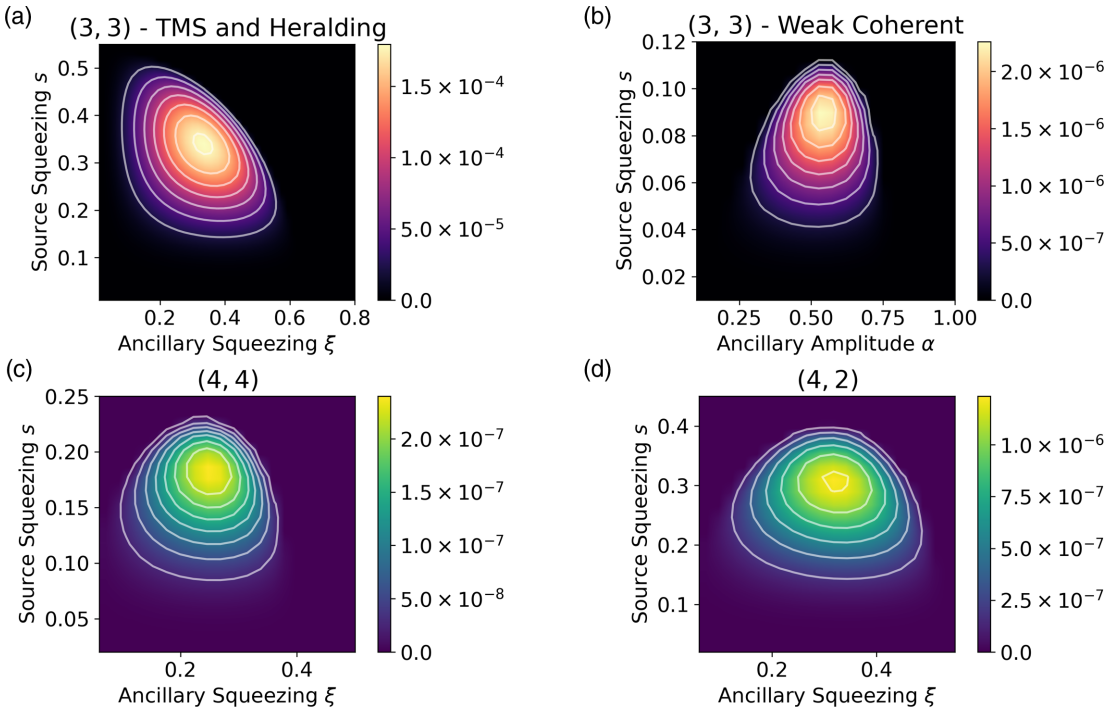

FIG. 3. Optimization of source and ancillary states parameters in the high-dimensional network. Color-coded are the secrets bits per round of the simultaneous subspace coding protocol in different configurations and for different values of sources squeezing (s) and ancillary parameters. (a) $d = 3$ and $k = 3$ using a heralded single photon from a TMS state, with squeezing ξ as the ancilla. (b) $d = 3$ and $k = 3$ using a weak coherent state, with amplitude α, for the ancilla. (c) $d = 4$ and $k = 4$ and (d) $d = 4$ and $k = 2$ using a TMS state with squeezing ξ for the ancillas.

for near-term networks where noises are expected to be significant.

Another typical experimental obstacle that will affect secret key rates in practical implementations is the finite efficiency of single-photon detectors (e.g., a typical value of superconductive single-photon detectors is around 90% and for noncryogenic single-photon detectors a typical value is 30% [35]). In a realistic network, imperfect detectors with efficiency $\eta < 1$ and channel noises, such as the ones studied above, are likely to happen simultaneously. It is thus import to analyze how the presence of both affect the quantum network performance. In Fig. 5 we report simulation results of the optimal rates as a function of the detector inefficiency $1 - \eta$ and for different values of the crosstalk parameter characterizing the channel noise. In the simulations, η is the probability that a threshold detector fails to herald the presence of one or more photons, which is considered to be uniform for all detectors. As expected, lower detector efficiency is always detrimental

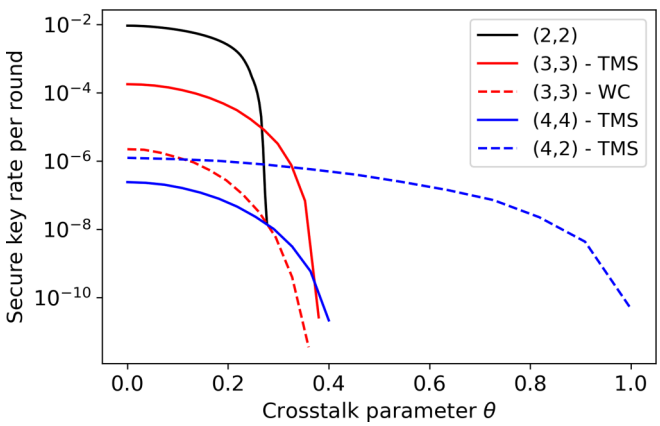

FIG. 4. Optimal secret key rates in noisy quantum networks. Represented are the secure bits per round using the simultaneous subspace coding protocol as a function of the cross-talk noise parameter θ. For each value of θ, the key rates are optimized over all source and ancillary squeezing and/or amplitude parameters.

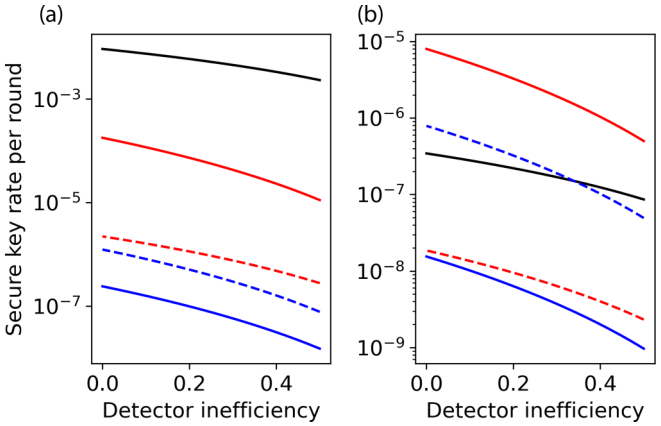

FIG. 5. Optimal key rates in noisy quantum networks with imperfect detectors. Secure bits per round against detector inefficiency $1 - \eta$, for two exemplary values of crosstalk noise values in the network: (a) $\theta = 0$, (b) $\theta = 0.272$. Plotted lines refer to the same legend as in Fig. 4.

for the secret key rates, and the effect is, in general, stronger when increasing the system dimensionality due to having to detect additional ancillary photons in the Bell measurement. This may imply that smaller dimensions can become favored when η gets too small, as shown in Fig. 5(b). Therefore, both experimental noise parameters η and θ can play an important role when determining the optimal dimensionality that maximizes secret key rates in a quantum network.

IV. CONCLUSIONS

Hi-D quantum states, in general, exhibit special properties especially useful in practical quantum technologies experiencing noisy environments. In this article, we investigated the possibility of creating a repeater-based quantum network with Hi-D states using state-of-the-art devices. We have studied the expected performance of Hi-D systems and compared them to the standard qubit approach. Furthermore, we have presented an alternative tool for processing high-dimensional quantum states, which is useful for low-dimensional spaces, i.e., $d < 5$ in which *ad hoc* quantum states can replace real single-photon sources for simplicity.

Our work represents a concrete study of a possible quantum network based on high-dimensional quantum repeaters, but open questions remain. For example, we expect that the success probability of the Hi-D Bell state measurements at the repeater stage, an important factor reducing Hi-D key rates, can be significantly improved considering additional heralding patterns resulting in high-dimensional entangled states. Besides, computer-aided design methods could be used to find more efficient schemes for Hi-D Bell state measurements [36].

Furthermore, in our analysis we focused on the robustness to operational noise in high-dimensional networks compared to the simple qubit case, but not considered loss correction. We point out that losses affect the key rates as in the qubit case and that quantum memories will thus be required in order to overcome the rate-distance limit [2]. The reduced success probability of Bell measurements in the Hi-D quantum repeaters means that longer coherence times for memories will be required. The improved noise robustness we showed here could compensate additional errors due to longer storage time. Further investigation on this point will thus require advances in Hi-D quantum memories, currently in their infancy [37–40].

Our results promise an advantage in using Hi-D quantum repeaters for QKD networks in noisy environments. The results could open a pathway for practical applications where environmental noise cannot be neglected. Clearly, more work in this direction is needed to find a realistic trade-off for repeater-based QKD networks among dimensionality, secure key rates, loss tolerance, and noise tolerance.

ACKNOWLEDGMENTS

The authors thank J. A. Adcock, B. Da Lio, D. Cozzolino, M. Krenn, and M. Malik for fruitful discussions. This work is supported by the Center of Excellence, SPOC-Silicon Photonics for Optical Communications (Grant No. DNRF123); the Hy-Q Center for Hybrid Quantum Networks (Grant No. DNRF 139); and the EraNET Cofund Initiatives QuantERA within the European Union's Horizon 2020 research and innovation program, Grant No. 731473 (Project SQUARE). M.H. acknowledges funding from the Austrian Science Fund (FWF) through START Project No. Y879-N27. M.E. acknowledges support from FWF Project No. W 1210-N25 (CoQuS).

APPENDIX A: DETAILED CALCULATIONS FOR THE CONTAINED INFORMATION IN THE Hi-D ENTANGLEMENT-SWAPPING PROCEDURE

We start with the ideal input state $|\psi\rangle_{\text{in}}^{\text{4d}}$ in the four-dimensional case without double-pair emissions or coherent states reading

$$\begin{aligned}|\psi\rangle_{\text{in}}^{\text{4d}} =& \frac{1}{16}(|0\rangle_c + |1\rangle_c + |2\rangle_c + |3\rangle_c)(|0\rangle_d + |1\rangle_d + |2\rangle_d + |3\rangle_d)\\ &(|0\rangle_a|0\rangle_e + |1\rangle_a|1\rangle_e + |2\rangle_a|2\rangle_e + |3\rangle_a|3\rangle_e)\\ &(|0\rangle_b|0\rangle_f + |1\rangle_b|1\rangle_f + |2\rangle_b|2\rangle_f + |3\rangle_b|3\rangle_f),\end{aligned} \tag{A1}$$

where photons a and f are to be entangled in this swapping process (see Fig. 2 and note that we slightly change notation such that $x_y \to |y-1\rangle_x$). Following the recipe given in Luo *et al.*, we apply an extended unitary transformation U_{4+1} on one of the entangled pairs, where we here choose photon b reading

$$\begin{aligned}|0\rangle_b &\to -2|0\rangle_b + |1\rangle_b + |2\rangle_b + |3\rangle_b + |4\rangle_b/2\sqrt{2},\\ |1\rangle_b &\to |0\rangle_b - 2|1\rangle_b + |2\rangle_b + |3\rangle_b + |4\rangle_b/2\sqrt{2},\\ |2\rangle_b &\to |0\rangle_b + |1\rangle_b - 2|2\rangle_b + |3\rangle_b + |4\rangle_b/2\sqrt{2},\\ |3\rangle_b &\to |0\rangle_b + |1\rangle_b + |2\rangle_b - 2|3\rangle_b + |4\rangle_b 2\sqrt{2},\\ |4\rangle_b &\to |0\rangle_b + |1\rangle_b + |2\rangle_b + |3\rangle_b - 2|4\rangle_b/2\sqrt{2},\end{aligned} \tag{A2}$$

and note that the input mode $|4\rangle_b$ is left empty or is not occupied and the output mode $|4\rangle_b$ is ignored. Hence, the extended unitary transformation U_{4+1} is not unitary in the subspace spanned by the modes $|0\rangle_b$, $|1\rangle_b$, $|2\rangle_b$, and $|3\rangle_b$.

The generalization of a usual beam-splitter utilized in two-dimensional entanglement swapping experiments, is the quantum Fourier transformation (QFT). In our case, the QFT is defined by

$$|m\rangle_p \to \frac{1}{\sqrt{d}} \sum_{k\in\{b,c,d,e\}} \exp\left[m\frac{2\pi i}{d}\Phi(p)\right]|m\rangle_k, \tag{A3}$$

where the mode m is constant and the sum is over all possible paths $k \in \{a, b, c, d\}$ in the four-dimensional case. The function $\Phi(p)$ describes a path-dependent phase assignment according to

$$\Phi(p) = \begin{cases} 0 \text{ for } p = a,\\ 1 \text{ for } p = c,\\ 2 \text{ for } p = d,\\ 3 \text{ for } p = b.\end{cases} \tag{A4}$$

Hence, the QFT does not change the incoming mode m, but mixes all modes from all inputs equally with relative phases depending on their mode m and input path p.

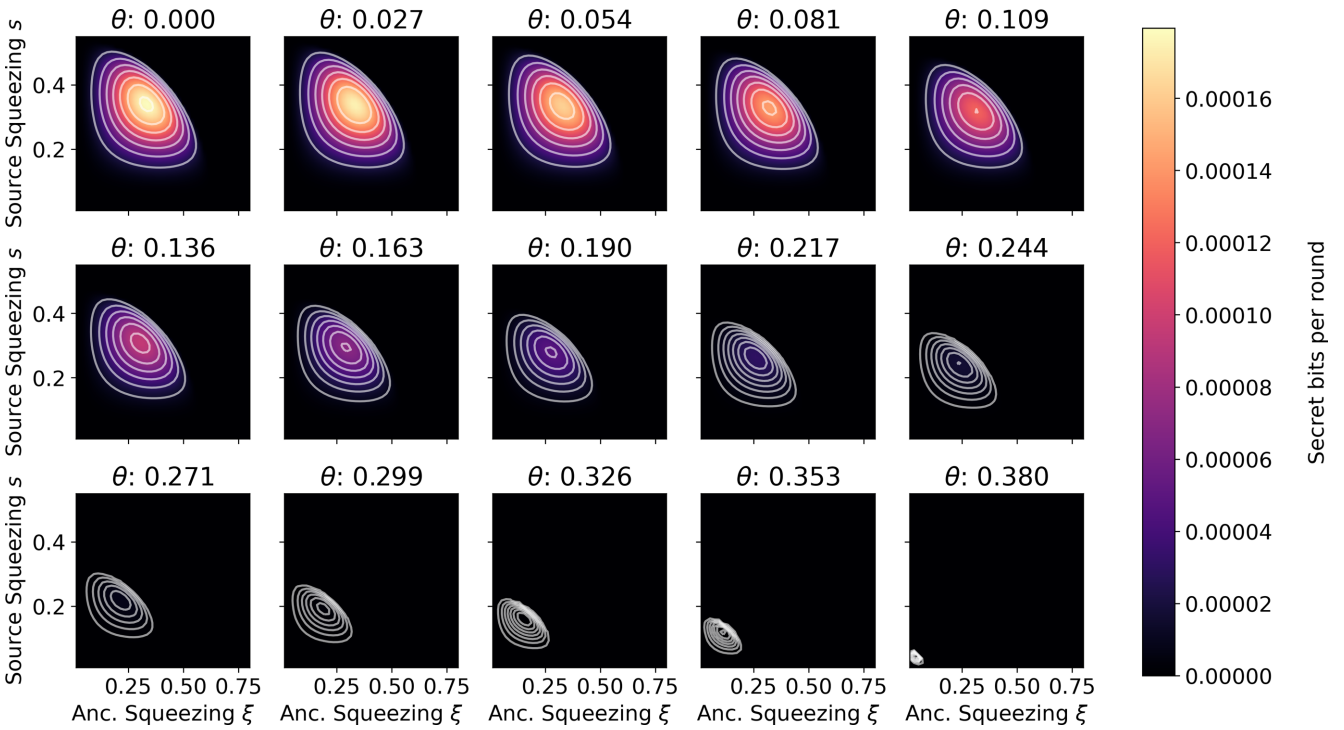

FIG. 6. Optimization of the source and ancillary squeezing parameters for different levels of crosstalk noise for the $d = 3$ and $k = 3$ case and ancillas from heralded TMS states.

We denote the output state after the extended unitary transformation $U^b_{4+1} = \mathbb{1}^{a,c,d,e,f} \otimes U^b_{4+1}$ on photon f, the cancellation $C^b_{m=4}$ of the additional mode $|4\rangle_b$ in path b, and the quantum Fourier transformation in four dimensions $\mathrm{QFT}_4^{a,c,b,d}$ on photons a, b, c, and d according to Eq. (A3) with

$$|\psi\rangle^{4\mathrm{d}}_{\mathrm{out}} = \mathrm{QFT}_4^{a,c,b,d} \cdot C^b_{m=4} \cdot U^b_{4+1} |\psi\rangle^{4\mathrm{d}}_{\mathrm{in}}. \tag{A5}$$

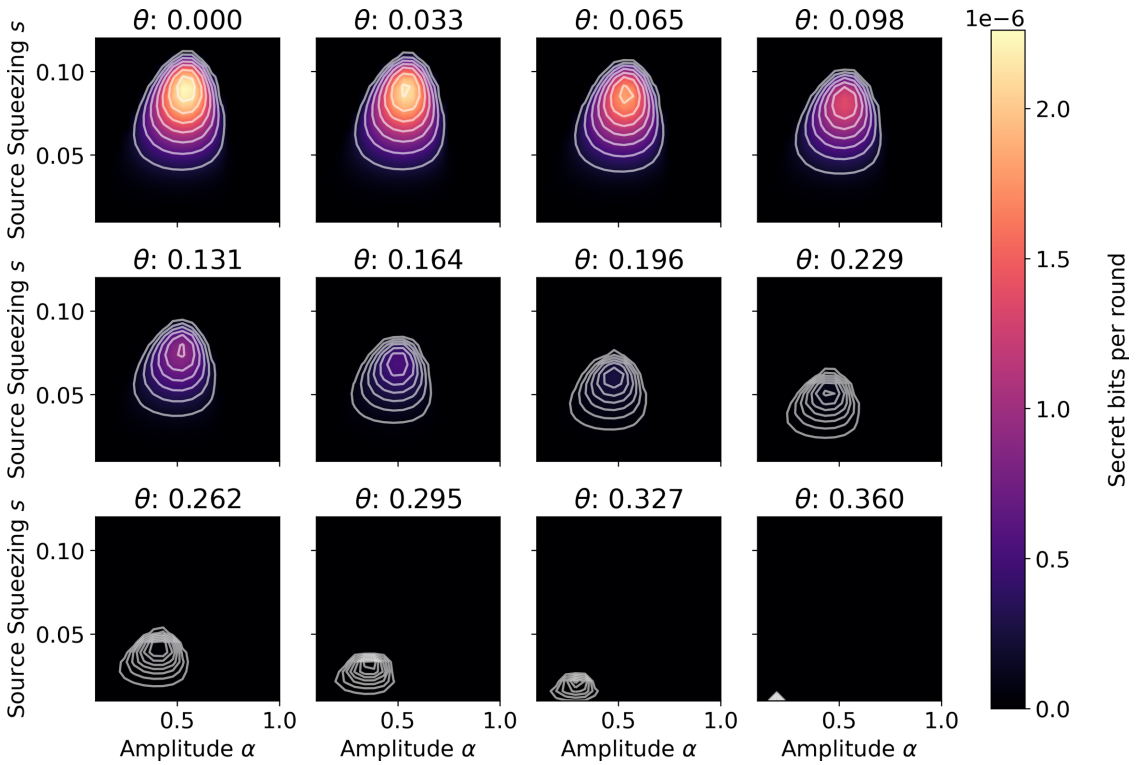

FIG. 7. Optimization of the source squeezing parameter and ancillary weak-coherent amplitude for different levels of crosstalk noise for the $d = 3$-$k = 3$ case and WC ancillas.

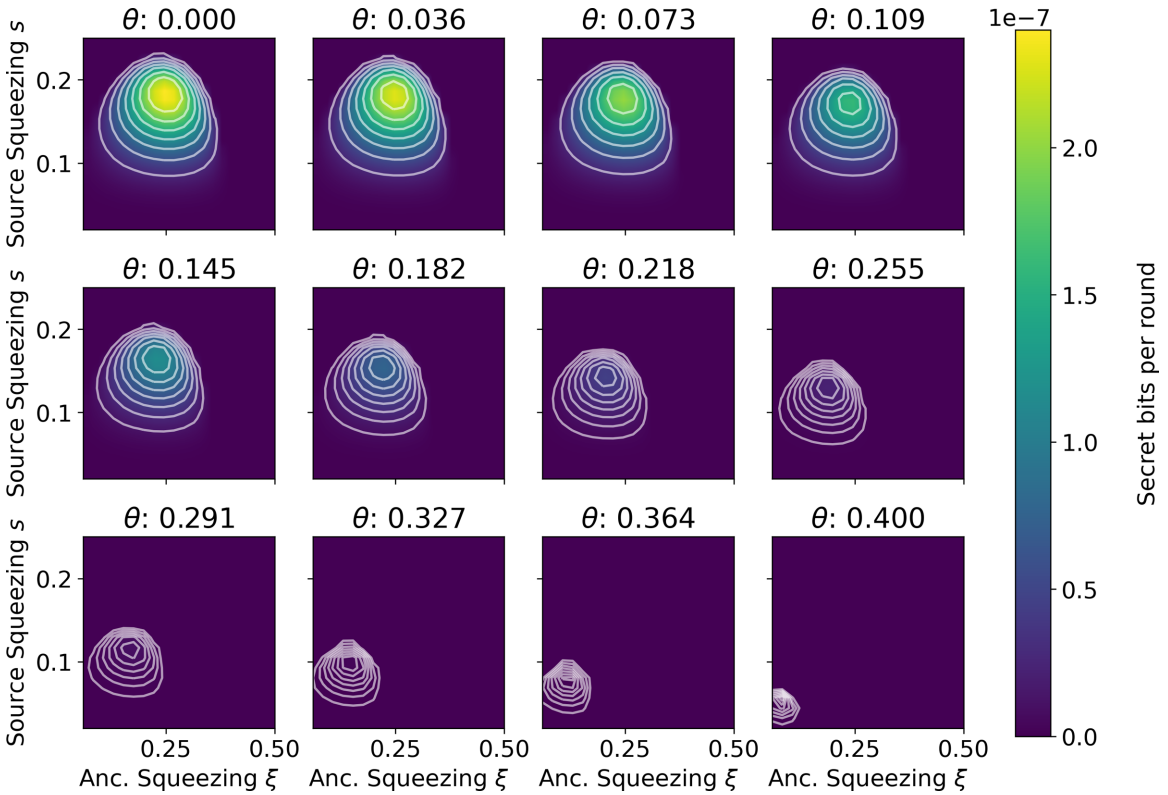

FIG. 8. Optimization of the source and ancillary squeezing parameters for different levels of cross-talk noise for the $d = 4$-$k = 4$ case.

The final step in the high-dimensional entanglement swapping protocol is to postselect on specific photon detection click-patterns. Mathematically, this is described by projecting onto specific modes for photons $\{a, b, c, d\}$ and then tracing out the detected photon space. Here, only projections into the space of four photons simultaneously are considered. An example for such a projection is to postselect only states that simultaneously triggered clicks in all b detectors, that is, to project onto the following subspace:

$$P(|0\rangle_b|1\rangle_b|2\rangle_b|3\rangle_b) = |0\rangle_b|1\rangle_b|2\rangle_b|3\rangle_b\langle 3|_b\langle 2|_b\langle 1|_b\langle 0|_b. \quad \text{(A6)}$$

The remaining state of photons e and f now reads

$$\begin{aligned}|\varphi\rangle_{\text{ef}} &= P(|0\rangle_b|1\rangle_b|2\rangle_b|3\rangle_b)|\psi\rangle_{\text{out}}^{\text{4d}} \\ &= \frac{3}{256\sqrt{2}}(|0\rangle_e|0\rangle_f + |1\rangle_e|1\rangle_f + |2\rangle_e|2\rangle_f + |3\rangle_e|3\rangle_f),\end{aligned} \quad \text{(A7)}$$

which describes a maximally entangled four-dimensional quantum state. The probability for this event to occur is given by $|_{\text{ef}}\langle\varphi|\varphi\rangle_{\text{ef}}|^2 = \frac{9}{8192}$. Hence, in approximately 1 of 1000 events this particular click-pattern is observed, which allows us to conclude that the entanglement swapping procedure was successful, and hence we can use it to utilize it in the quantum key distribution protocol. Fortunately, there exist more click-patterns that lead to a successful swapping protocol. Specifically, all click-patterns

$$p(i)[m1] \times p(j)[m2] \times p(k)[m3] \times p(l)[m4] \quad \text{(A8)}$$

where $m1$ to $m4$ are elements of $\{0, 1, 2, 3\}$ and describe the modes that fulfill $m1 \neq m2 \neq m3 \neq m4$ are valid click-patterns. The paths $p(i)$, $p(j)$, $p(k)$, and $p(l)$ can take any value according to

$$p(x) = \begin{cases} b & \text{for } x = 1, \\ c & \text{for } x = 2, \\ d & \text{for } x = 3, \\ e & \text{for } x = 4. \end{cases} \quad \text{(A9)}$$

In total there exist 192 valid click-patterns. Not all click-patterns occur with the same probability and or lead to maximally entangled states. To account for this, we calculate the probability for each click-pattern to occur and also the von Neumann entropy of the reduced density matrix, that is,

$$S\big(\rho_a^{(i)}\big) = -\text{Tr}\big[\rho_a^{(i)} \ln(\rho_a^{(i)})\big], \quad \text{(A10)}$$

where $\rho_a^{(i)}$ describes the reduced density matrix of photon a for the observed click-pattern (i) only:

$$\rho_a^{(i)} = \text{Tr}_f\big(|\varphi\rangle_{af}^{(i)}\langle\varphi|\big). \quad \text{(A11)}$$

Finally, we calculate the contained information I of the swapping procedure as the sum over all 192 click-patterns (i) of the product of the occurrence probability and the contained information, according to

$$I = \sum_{i=1}^{192} |\langle\varphi^{(i)}|\varphi^{(i)}\rangle|^2 \cdot S\big(\rho_a^{(i)}\big), \quad \text{(A12)}$$

and this leads in the four-dimensional case to 0.07945 bits.

Repeating and adapting the above steps described from Eq. (A1) to Eq. (A12) for the two-dimensional case and the three-dimensional case results in

$$I(d = 2) = 0.5 \text{ bits}, \quad I(d = 3) = 0.184 \text{ bits}. \quad \text{(A13)}$$

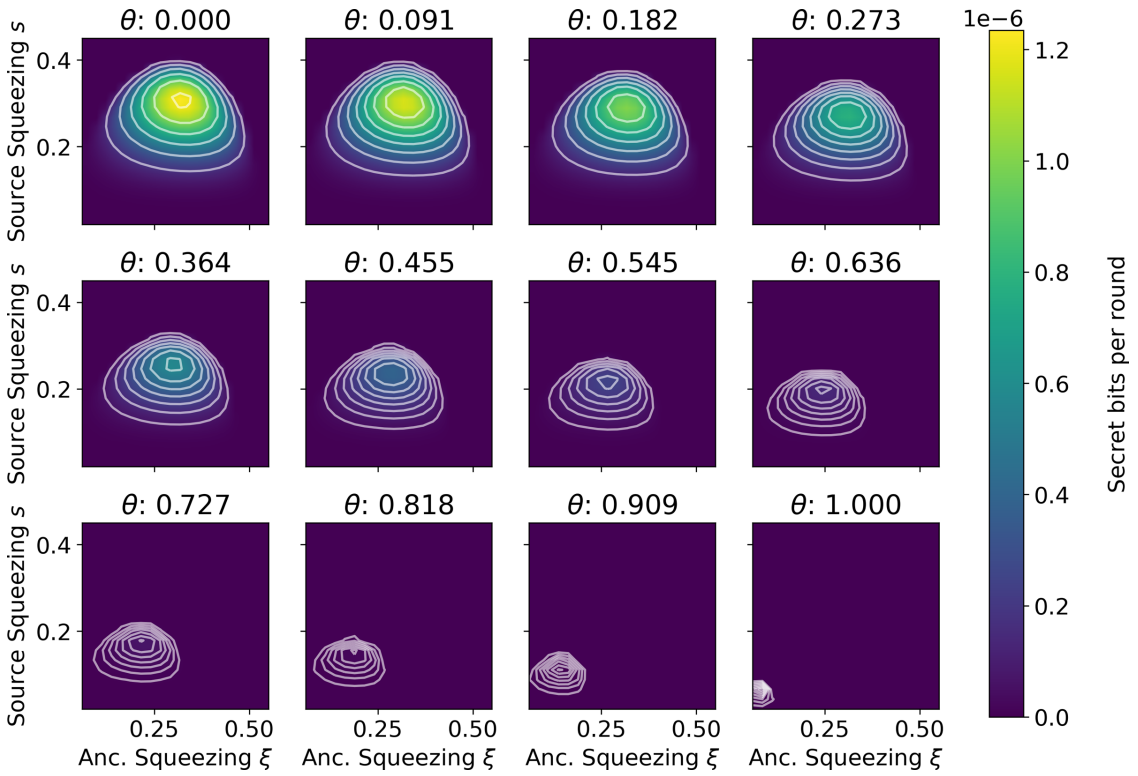

FIG. 9. Optimization of the source and ancillary squeezing parameters for different levels of cross-talk noise for the $d = 4$-$k = 2$ case.

APPENDIX B: OPTIMIZATION OF SQUEEZING AND AMPLITUDE PARAMETERS FOR DIFFERENT LEVELS OF NOISE

As discussed in the main text, for different levels of noise due to crosstalk, dark counts, and losses, the optimal squeezing and amplitude parameters for Alice's and Bob's sources or the ancillary sources will change. In Figs. 6–9 this change is shown explicitly for the crosstalk type of noise and for the different type of high-dimensional configurations investigated in the main text.

[1] J. Preskill, Quantum computing in the NISQ era and beyond, Quantum **2**, 79 (2018).

[2] S. Pirandola, U. L. Andersen, L. Banchi, M. Berta, D. Bunandar, R. Colbeck, D. Englund, T. Gehring, C. Lupo, C. Ottaviani *et al.*, Advances in quantum cryptography, Adv. Opt. Photonics **12**, 1012 (2020).

[3] A. Boaron, G. Boso, D. Rusca, C. Vulliez, C. Autebert, M. Caloz, M. Perrenoud, G. Gras, F. Bussières, M.-J. Li *et al.*, Secure Quantum Key Distribution over 421 km of Optical Fiber, Phys. Rev. Lett. **121**, 190502 (2018).

[4] M. Minder, M. Pittaluga, G. L. Roberts, M. Lucamarini, J. Dynes, Z. Yuan, and A. Shields, Experimental quantum key distribution beyond the repeaterless secret key capacity, Nat. Photonics **13**, 334 (2019).

[5] D. Bacco, B. Da Lio, D. Cozzolino, F. Da Ros, X. Guo, Y. Ding, Y. Sasaki, K. Aikawa, S. Miki, H. Terai *et al.*, Boosting the secret key rate in a shared quantum and classical fibre communication system, Commun. Phys. **2**, 1 (2019).

[6] H.-L. Yin, T.-Y. Chen, Z.-W. Yu, H. Liu, L.-X. You, Y.-H. Zhou, S.-J. Chen, Y. Mao, M.-Q. Huang, W.-J. Zhang *et al.*, Measurement-Device-Independent Quantum Key Distribution over a 404 km Optical Fiber, Phys. Rev. Lett. **117**, 190501 (2016).

[7] S. Paesani, Y. Ding, R. Santagati, L. Chakhmakhchyan, C. Vigliar, K. Rottwitt, L. K. Oxenløwe, J. Wang, M. G. Thompson, and A. Laing, Generation and sampling of quantum states of light in a silicon chip, Nat. Phys. **15**, 925 (2019).

[8] I. M. Georgescu, S. Ashhab, and F. Nori, Quantum simulation, Rev. Mod. Phys. **86**, 153 (2014).

[9] D. P. Divincenzo, *Topics in Quantum Computers*, edited by L. L. Sohn, L. P. Kouwenhoven, and G. Schön, Mesoscopic Electron Transport, NATO ASI Series (Series E: Applied Sciences), Vol 345 (Springer, Dordrecht, 1997), pp. 657–677.

[10] S. Wehner, D. Elkouss, and R. Hanson, Quantum internet: A vision for the road ahead, Science **362**, eaam9288 (2018).

[11] Y. Zhong, H.-S. Chang, A. Bienfait, É. Dumur, M.-H. Chou, C. R. Conner, J. Grebel, R. G. Povey, H. Yan, D. I. Schuster, and A. N. Cleland, Deterministic multi-qubit entanglement in a quantum network, Nature (London) **590**, 571 (2021).

[12] T. Northup and R. Blatt, Quantum information transfer using photons, Nat. Photonics **8**, 356 (2014).

[13] W. K. Wootters and W. H. Zurek, A single quantum cannot be cloned, Nature (London) **299**, 802 (1982).

[14] H.-J. Briegel, W. Dür, J. I. Cirac, and P. Zoller, Quantum Repeaters: The Role of Imperfect Local Operations in Quantum Communication, Phys. Rev. Lett. **81**, 5932 (1998).

[15] W. J. Munro, A. M. Stephens, S. J. Devitt, K. A. Harrison, and K. Nemoto, Quantum communication without the necessity of quantum memories, Nat. Photonics **6**, 777 (2012).

[16] S. Muralidharan, J. Kim, N. Lütkenhaus, M. D. Lukin, and L. Jiang, Ultrafast and Fault-Tolerant Quantum Communication across Long Distances, Phys. Rev. Lett. **112**, 250501 (2014).

[17] S. Muralidharan, L. Li, J. Kim, N. Lütkenhaus, M. D. Lukin, and L. Jiang, Optimal architectures for long distance quantum communication, Sci. Rep. **6**, 20463 (2016).

[18] M. Zukowski, A. Zeilinger, M. A. Horne, and A. K. Ekert, "Event-Ready-Detectors" Bell Experiment via Entanglement Swapping, Phys. Rev. Lett. **71**, 4287 (1993).

[19] D. Cozzolino, B. Da Lio, D. Bacco, and L. K. Oxenløwe, High-dimensional quantum communication: Benefits, progress, and future challenges, Adv. Quantum Technol. **2**, 1900038 (2019).

[20] S. Ecker, F. Bouchard, L. Bulla, F. Brandt, O. Kohout, F. Steinlechner, R. Fickler, M. Malik, Y. Guryanova, R. Ursin *et al.*, Overcoming Noise in Entanglement Distribution, Phys. Rev. X **9**, 041042 (2019).

[21] M. Erhard, M. Krenn, and A. Zeilinger, Advances in high-dimensional quantum entanglement, Nat. Rev. Phys. **2**, 365 (2020).

[22] D. Cozzolino, D. Bacco, B. Da Lio, K. Ingerslev, Y. Ding, K. Dalgaard, P. Kristensen, M. Galili, K. Rottwitt, S. Ramachandran *et al.*, Orbital Angular Momentum States Enabling Fiber-Based High-Dimensional Quantum Communication, Phys. Rev. Appl. **11**, 064058 (2019).

[23] J. Calsamiglia, Generalized measurements by linear elements, Phys. Rev. A **65**, 030301 (2002).

[24] Y.-H. Luo, H.-S. Zhong, M. Erhard, X.-L. Wang, L.-C. Peng, M. Krenn, X. Jiang, L. Li, N.-L. Liu, C.-Y. Lu *et al.*, Quantum Teleportation in High Dimensions, Phys. Rev. Lett. **123**, 070505 (2019).

[25] X.-M. Hu, C. Zhang, B.-H. Liu, Y. Cai, X.-J. Ye, Y. Guo, W.-B. Xing, C.-X. Huang, Y.-F. Huang, C.-F. Li *et al.*, Experimental High-Dimensional Quantum Teleportation, Phys. Rev. Lett. **125**, 230501 (2020).

[26] J. Wang, S. Paesani, Y. Ding, R. Santagati, P. Skrzypczyk, A. Salavrakos, J. Tura, R. Augusiak, L. Mančinska, D. Bacco *et al.*, Multidimensional quantum entanglement with large-scale integrated optics, Science **360**, 285 (2018).

[27] F. Kaneda and P. G. Kwiat, High-efficiency single-photon generation via large-scale active time multiplexing, Sci. Adv. **5**, eaaw8586 (2019).

[28] C. Weedbrook, S. Pirandola, R. García-Patrón, N. J. Cerf, T. C. Ralph, J. H. Shapiro, and S. Lloyd, Gaussian quantum information, Rev. Mod. Phys. **84**, 621 (2012).

[29] C. S. Hamilton, R. Kruse, L. Sansoni, S. Barkhofen, C. Silberhorn, and I. Jex, Gaussian Boson Sampling, Phys. Rev. Lett. **119**, 170501 (2017).

[30] N. Quesada, J. M. Arrazola, and N. Killoran, Gaussian boson sampling using threshold detectors, Phys. Rev. A **98**, 062322 (2018).

[31] J. Bulmer, R. Chadwick, S. Paesani *et al.*, Threshold detector statistic of bosonic states (unpublished).

[32] M. Doda, M. Huber, G. Murta, M. Pivoluska, M. Plesch, and C. Vlachou, Quantum Key Distribution Overcoming Extreme Noise: Simultaneous Subspace Coding Using High-Dimensional Entanglement, Phys. Rev. Appl. **15**, 034003 (2021).

[33] X.-M. Hu, C. Zhang, Y. Guo, F.-X. Wang, W.-B. Xing, C.-X. Huang, B.-H. Liu, Y.-F. Huang, C.-F. Li, G.-C. Guo, X. Gao, M. Pivoluska, and M. Huber, Pathways for Entanglement-Based Quantum Communication in the Face of High Noise, Phys. Rev. Lett. **127**, 110505 (2021).

[34] G. Rademacher, R. S. Luís, B. J. Puttnam, Y. Awaji, and N. Wada, Crosstalk dynamics in multi-core fibers, Opt. Express **25**, 12020 (2017).

[35] M. D. Eisaman, J. Fan, A. Migdall, and S. V. Polyakov, Invited review article: Single-photon sources and detectors, Rev. Sci. Instrum. **82**, 071101 (2011).

[36] M. Krenn, M. Erhard, and A. Zeilinger, Computer-inspired quantum experiments, Nat. Rev. Phys. **2**, 649 (2020).

[37] V. Parigi, V. D'Ambrosio, C. Arnold, L. Marrucci, F. Sciarrino, and J. Laurat, Storage and retrieval of vector beams of light in a multiple-degree-of-freedom quantum memory, Nat. Commun. **6**, 1 (2015).

[38] D.-S. Ding, W. Zhang, S. Shi, Z.-Y. Zhou, Y. Li, B.-S. Shi, and G.-C. Guo, High-dimensional entanglement between distant atomic-ensemble memories, Light Sci. Appl. **5**, e16157 (2016).

[39] C. Li, Y.-K. Wu, W. Chang, S. Zhang, Y.-F. Pu, N. Jiang, and L.-M. Duan, High-dimensional entanglement between a photon and a multiplexed atomic quantum memory, Phys. Rev. A **101**, 032312 (2020).

[40] A. Tiranov, S. Designolle, E. Z. Cruzeiro, J. Lavoie, N. Brunner, M. Afzelius, M. Huber, and N. Gisin, Quantification of multi-dimensional entanglement stored in a crystal, Phys. Rev. A **96**, 040303 (2017).